JOURNAL OF GEOPHYSICAL RESEARCH, VOL. 103, NO. E11, PAGES 25,851–25,864, OCTOBER 25, 1998

Mapping the Martian polar ice caps: Applications of terrestrial optical remote sensing methods

Anne W. Nolin
National Snow and Ice Data Center, University of Colorado, Boulder

Abstract. With improvements in both instrumentation and algorithms, methods for mapping terrestrial snow cover using optical remote sensing data have progressed significantly over the past decade. Multispectral data can now be used to determine not only the presence or absence of snow but the fraction of snow cover in a pixel. Radiative transfer models have been used to quantify the nonlinear relationship between surface reflectance and grain size thereby providing the basis for mapping snow grain size from surface reflectance images. Model-derived characterization of the bidirectional reflectance distribution function provides the means for converting measured bidirectional reflectance to directional-hemispherical albedo. In recent work, this approach has allowed climatologists to examine the large scale seasonal variability of albedo on the Greenland ice sheet. This seasonal albedo variability results from increases in snow grain size and exposure of the underlying ice cap as the seasonal snow cover ablates away. With the current Mars Global Surveyor and future missions to Mars, it will soon be possible to apply some of these terrestrial mapping methods to learn more about Martian ice properties, extent, and variability. Distinct differences exist between Mars and Earth ice mapping conditions, including surface temperature, ice type, ice-mineral mixtures, and atmospheric properties, so a direct application of terrestrial snow and ice mapping methods may not be possible. However, expertise in mapping and interpreting terrestrial snow and ice will contribute to the inventory of techniques for mapping planetary ices. Furthermore, adaptation of terrestrial methods will provide a basis for comparison of terrestrial and planetary cryospheric components.

1. Comparison Between Ices on Earth and Mars

In comparative planetology, we often look at similarities between Earth and Mars. One of the most striking features of both planets, with critical linkages to climate change and hydrology, is the existence of large ice caps in their polar regions. Earth's cryosphere can, in some ways, serve as an analog for the Martian ice. Compared with Earth, we have only a limited set of remote sensing observations for the Martian polar caps. Future Mars missions and continued advancements in instrumentation and algorithms will enhance our abilities to compare and understand terrestrial and Martian polar regions.

While we know terrestrial snow to be highly reflecting in the visible part to the spectrum, in the near-infrared wavelengths its albedo ranges from about 0.8 to near zero (see Fig. 1). Unlike most other surface cover types, snow and ice have extreme spectral variability over a span of only 2 μm. In comparison to Martian temperature regimes, ice on Earth exists in a state that is close to the melting point. Seasonal insolation differences lead to substantial variability of snow cover, sea ice, and ice sheet conditions extent over the course of a year. Over Earth's northern hemisphere, seasonal extremes of snow and ice cover range from a January maximum of about 23% to an August minimum of 3% [*Barry*, 1985], with significant regional and interannual variability in most months [*Robinson and Dewey*, 1990]. It is this combination of spectral, spatial, and temporal variability that makes snow and ice the most dynamic of Earth's surface cover types.

Although surface temperatures are typically colder than those found on Earth, the polar regions of Mars still experience changes in frost-covered area, surface albedo and sublimation rates [*Kieffer et al.*, 1976; *Farmer et al.*, 1976; *Paige and Ingersoll*, 1985; *Haberle and Jakosky*, 1990]. On Mars, the extent of ice is less well-known and may extend into the lower latitudes as ground ice [*Paige*, 1992; *Mellon and Jakosky*, 1995]. *Mellon and Jakosky*, [1995] showed that ground ice is stable on Mars at latitudes greater than 60° and that ice may be present near the surface. Thermal models and observations of polygonal features also show that ground ice may be present at lower latitudes during periods of high obliquity of the Martian orbit [*Mel-*

Copyright 1998 by the American Geophysical Union.

Paper number 98JE02082.
0148-0227/98/98JE-02082$09.00

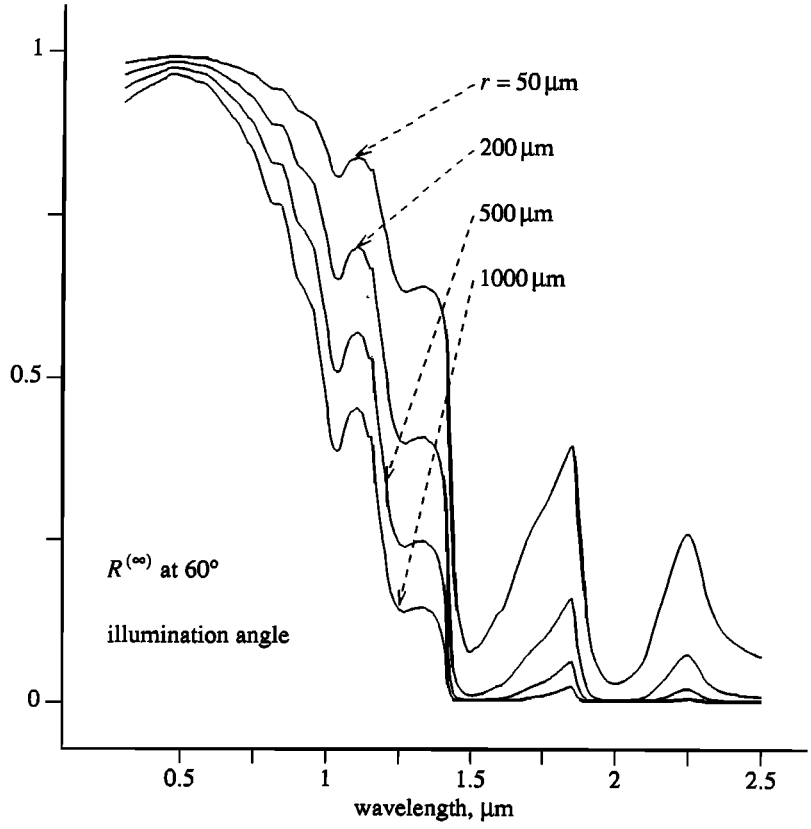

Figure 1. Modeled directional-hemispherical spectral reflectances of snow for different optically equivalent grain radii.

lon et al., 1997]. Studies of terrestrial permafrost may shed light on the dynamics and distribution of Martian ground ice.

As with Earth's fresh water, most Martian water resides in the polar regions in the form of ice caps. While both the northern and southern Mars polar caps are bright compared with non-ice covered regions, the compositions of the ice caps differ. The more extensive north polar cap consists of H_2O ice and the smaller south polar cap is thought to be mostly or entirely CO_2 ice [*Kieffer et al.*, 1976; *Farmer et al.*, 1976]. Modeling and observational evidence support the idea of little, if any, CO_2 in the northern hemisphere permanent ice cap [*Mellon*, 1996; *Clark and McCord*, 1982].

Polar and ground ice are thought to be important components of the Martian hydrologic cycle where sublimation processes dominate the ice-atmosphere interactions [*Haberle and Jakosky*, 1990, *Mellon and Jakosky*, 1995]. Measurements of Martian atmospheric water vapor show large changes in water vapor amounts through the course of a year [*Jakosky and Farmer*, 1982] and that the north polar cap is a likely source [*Haberle and Jakosky*, 1990].

A significant difference between Martian and terrestrial ices is the amount of light absorbing particulates in the Martian polar ice caps and seasonal frost deposits. Dust is a significant component of Martian ice, with roughly equal parts of dust and water present in the layered terrains and unknown quantity of dust in the north polar cap [*Kieffer*, 1990]. *Clark and McCord*, [1982] modeled the reflectance spectrum of the polar cap surface using a linear mixture of 60% medium-grained water frost and 40% clay minerals. They estimated that the permanent cap could contain 10-40% by weight of mineral particulates. The seasonal cycle of CO_2 deposition is also affected by Martian dust. Atmospheric dust is removed as CO_2 condenses on dust particles and precipitates onto the ice cap surface. These dust particles remain in the seasonal surface deposits and are thought to control both surface albedo and sublimation rates [*Pollack et al.*, 1990]. This is a different case than for Earth's polar caps that are nearly pure ice with generally less than 0.5 ng/g elemental carbon [*Warren and Clarke*, 1990] and less than 26 ng/g dust [*Kumai*, 1976; *Royer et al.*, 1983]. Changes in surface albedo and energy balance for terrestrial ice sheets are primarily driven by changes in surface snow grain size [*Nolin and Stroeve*, 1997]. Thus comparisons between Earth and Martian ice-atmosphere interactions are not straightforward.

2. Some Relevant Martian Ice Mapping Questions

What is similar between Earth and Mars is that their extensive ice caps appear to record, respond to, and per-

turb climate change. On Earth, polar ice coring efforts have generated a climate time series extending back over 110,000 years. These data document changes in Earth climate driven by periodic variability in Earth-Sun geometry [*Johnsen et al.*, 1997; *Yang et al.*, 1997] as well as other, shorter-term fluctuations [*Barlow et al.*, 1993; *White et al.*, 1997]. Other ongoing polar climatological investigations are examining changes in ice sheet elevation, ice flow, calving rates, surface energy balance, and snow accumulation rates over the ice sheets. These short-timescale variations, involving ice-ocean-atmosphere interactions, are not well-quantified.

The salient questions on Mars are in some ways more exploratory in nature. For instance, although the Mariner 9 and Viking Orbiter 2 have provided images of Mars' polar regions, the exact composition of each polar cap remains somewhat obscured. Changes in ice extent have been difficult to quantify because of lack of multispectral image data. Mapping ice extent and polar layered deposits is key to understanding long term changes in Martian climate that are thought to be driven by quasi-periodic orbital variations [*Howard et al.*, 1982].

On shorter timescales, the spatial extent and temporal variability of CO_2 frost deposition and sublimation on the polar caps are not well-characterized. A 25% decrease in apparent albedo (uncorrected for anisotropic scattering) most likely indicates the seasonal removal of the CO_2 surface frost from the north polar ice cap [*Paige and Ingersoll*, 1985]. The CO_2 frost sublimation dynamics need to be quantified, since the latent heat of CO_2 frost sublimation is a significant component in the heat budget for the polar caps [*Paige and Ingersoll*, 1985]. Determination of surface frost grain sizes and grain size metamorphism rates would provide clues to the thermodynamics of that process [*Clark et al.*, 1983]. Without more quantifiable information on ice extent, surface albedo, surface grain size, and dust content, it is difficult to characterize the interactions between the dusty Martian atmosphere and the polar ice caps.

Martian ground ice, while an important element of the global hydrologic cycle, is less amenable to direct observation by remote sensing instruments. In most cases, the overlying ice-free regolith obscures the buried soil layers, whose pores contain water ice. However, indirect evidence can be obtained through mapping polygonal features thought to be associated with seasonally driven frost heaving [*Mellon*, 1997]. These polygonal features may not represent present ground ice distributions, since they can persist for long periods. Although attempts to directly map Martian ground ice with remotely sensed data have not proven highly useful, geomorphic mapping at higher image resolution should help in their characterization.

To assess the applicability of optical remote sensing techniques to Martian ice mapping problems, an overview of these terrestrial methods is presented. This is followed by a discussion of how such methods might be applied to help answer some of the relevant questions about Martian ice.

3. Terrestrial Snow Mapping Using Optical Remote Sensing

In this section, selected snow/ice mapping methods are described. These optical remote sensing methods address mapping snow/ice extent, grain size and albedo and thus are considered candidates for adaptation to Martian ice cap mapping endeavors. It should be noted that passive microwave and radar techniques are widely used to map snow and ice on Earth. However, because such instrumentation has not been used in Mars mapping, and are not currently planned, the focus of this article is on the use of optical remote sensing methods.

As background, a brief overview of the optical properties of snow is given. However, for more detail on this subject, the reader is referred to the more comprehensive work of *Warren*, [1982].

3.1. Optical Properties of Snow

It is well known that the optical properties of ice can be directly related to snowpack physical properties such as grain size and albedo. An aggregation of ice particles will reflect nearly all energy in the visible wavelengths (0.4 - 0.7 μm) [*Wiscombe and Warren*, 1980]. In the visible, ice particles reflect predominantly into the forward direction. When light absorbing particulates (e.g. dust) are mixed with snow, reflectance decreases and becomes more isotropic [*Warren and Wiscombe*, 1980]. In the near-infrared region (0.7 - 2.5 μm), ice is still forward scattering but the property controlling the magnitude of albedo is the particle size [*Wiscombe and Warren*, 1980; *Warren*, 1982]. In Figure 1, results of a two-stream radiative transfer model demonstrate the relationship between spectral albedo and snow grain radius. Because a significant proportion of incident solar radiation is in the near-infrared region, grain-size-induced changes in albedo have important consequences for the surface radiation balance and top-of-atmosphere fluxes.

3.2. Optical Remote Sensing of Snow on Earth

Instrumentation available to map snow and ice on Earth differs greatly from the few instruments available for Mars. While optical remote sensing of Martian ice is currently limited, the following descriptions of terrestrial optical remote sensing techniques and instrumentation are meant to provide background and impetus for potential applications of terrestrial methods. While not exhaustive, this section provides a brief overview of the most widely used optical instruments for snow/ice mapping as well as selected methods that potentially could be used for mapping Martian ice cap surface characteristics.

The Landsat Thematic Mapper (TM), with 30 m spatial resolution and six channels in the visible and near-infrared, provides effective multispectral snow mapping capabilities (see Table 1) [*Dozier*, 1989*a*; *Hall et al.*, 1995; *Rosenthal and Dozier*, 1996]. The Advanced Very High Resolution Radiometer (AVHRR) has visible, near-infrared, and thermal channels and spatial res-

Table 1. Landsat Thematic Mapper Spectral Bands

Band Number	Spectral Range, μm
1	0.45 - 0.52
2	0.52 - 0.60
3	0.63 - 0.69
4	0.76 - 0.90
5	1.55 - 1.75
6	10.40 - 12.50
7	2.08 - 2.35

Band 1 was not used in this analysis because it tends to saturate over snow. Band 6 was not used because it is outside of the optical region.

olutions of 1 km and 4 km. The visible (0.58 - 0.68 μm) and near-infrared (0.725 - 1.10 μm) channels have been successfully used for mapping snow albedo over the Greenland ice sheet [*Stroeve et al.*, 1997]. With the upcoming launch of NASA's EOS AM-1 satellite, the Moderate Resolution Imaging Spectroradiometer (MODIS) sensor will have 19 channels in the visible and near-infrared (36 channels total) and a spatial resolution ranging from 250 m to 1 km. In addition to these existing and planned satellite-based optical sensors, airborne optical mapping delivers high spatial resolution and, in many cases, offers sensor types not yet available on satellite platforms. For example, the Airborne Visible/Infrared Imaging Spectrometer (AVIRIS) is an airborne imaging spectrometer with 224 spectral bands from 0.4 to 2.45 μm with a nominal sampling interval and spectral response function (full width at half maximum) of 10 nm. This instrument provides us with the appropriate band locations and spectral resolution for sensitivity to ice absorption features in the near-infrared wavelengths. In the following sections, methods using these optical instruments are described for mapping snow-covered area, snow grain size, and snow albedo.

3.3. Mapping Snow Covered Area

3.3.1. Binary snow/ice mapping. A binary classification is one in which each image pixel is designated as either 100% or 0% of a particular land cover component, in this case, snow. Such index-based classification methods are commonly used for mapping snow-covered area with multispectral optical remote sensing data. For instance, the Normalized Difference Snow Index (NDSI) has been chosen for the MODIS snow mapping algorithm [*Hall et al.*, 1995]. Unlike most land surface covers, snow is highly reflecting in the visible and only moderately reflecting in the near-infrared wavelengths. The NDSI uses a visible channel (0.52 - 0.60 μm) and a near-infrared channel (1.55 - 1.75 μm) in the following relationship:

$$\mathrm{NDSI} = (\mathrm{Vis} - \mathrm{NIR})/(\mathrm{Vis} + \mathrm{NIR}) \quad (1)$$

The normalization process is highly effective in reducing differences in irradiance conditions across an image. *Dozier and Marks*, [1987] developed an index-based method to map snow in the Sierra Nevada of California using Landsat (TM) bands 2 and 5 (see Table 1). *Dozier*, [1989a] found that a threshold value of 0.4 could discriminate snow from non-snow-covered pixels and most cloud-covered pixels. They also found that, by using a reflectance threshold of 11% in TM band 4, snow and open water could be separated.

Though its simplicity is appealing for computational reasons, several problems have plagued this two-band classification method. Index-based methods typically have difficulty distinguishing between snow and cirrus clouds because of their similar optical properties in both the visible and near-infrared. A separate cloud mask can be used that incorporates a spectral band centered at 1.6 μm (useful for mapping very small ice particles such as those in cirrus clouds). Shadowed snow is often misclassified as non-snow covered. Partially snow covered pixels can also be difficult to classify using a binary classification. It remains unclear what fraction, depth, and pattern of partial snow cover is needed in order for a pixel to be mapped as snow.

3.3.2. "Subpixel" snow mapping. The field of view of a sensor often contains more than one land surface cover type, causing "mixed pixels." For instance, in many regions, snow is typically spatially associated with rock and vegetation. Melting snow, even in topographically uniform regions, tends to be patchy [*Shook et al.*, 1993] revealing the underlying vegetation and soil. For hydrologic purposes and for estimating the thermodynamic state of the snowpack, we require knowledge of only the snow properties but not those of the other components that may be present in the pixel. We also require an accurate estimate of the fraction of a pixel that is covered by snow as a validation and calibration for the more widely used binary classification methods.

Spectral mixture analysis (SMA) is a multispectral method that is currently used for determining the fraction of snow cover in a pixel. This fractional snow mapping approach is termed "subpixel" mapping because it provides information on snow content in a pixel. This approach does not map the distribution of snow cover within a pixel, rather the contribution of the snow to the multispectral reflectance of the whole pixel. SMA evolved out of earlier research that relied on principal components analysis (PCA) to quantify the amounts of various constituents in chemical mixtures [*Lawton and Sylvestre*, 1971]. Mixture analysis was developed to analyze linear combinations of land surface covers having a adjacent (rather than a layered) spatial distribution [*Adams et al.*, 1986]. When incident photons interact with a single constituent before scattering, the spectral mixing process is described as predominantly linear. When light interacts with two or more materials before being reflected from the surface, this results in nonlinear spectral mixing. If the nature of the nonlinearity can be characterized [*Roberts et al.*, 1993] or if their properties can be linearized by using the single scattering albedo instead of single constituent reflectances [*Mustard and Pieters*, 1989; *Clark and Roush*, 1984], nonlinear mixing does not present a problem. Sources of nonlinearity

include intimate mixtures of mineral particulates and ice, optically thin snow, a wide range of mean snow grain size across the surface of a pixel, and changes in the spectral composition of irradiance over a pixel. The first of these nonlinear effects would have the largest effect for Martian frost/ice remote sensing. Though dust amounts in Earth snow are generally low, *Clark and Lucey*, [1984] have shown that higher dust particle concentrations, such as those that would be found on Mars, nonlinearly affect reflectance of mixtures.

The reflectance of an image pixel holds information about the number of constituents in a pixel, their spectral signatures, and their relative abundances. Such image constituents are termed "end-members" and each end-member is considered to be a pure representation of a surface cover type in the image (such as snow, rock, or vegetation). Each image can be well-represented by a finite and small set of spectrally-unique end-members that describes the dimensionality of the data [*Gillespie et al.*, 1990]. For a multispectral image, a linear mixture of the end-members is calculated using the following mixing rule [*Adams et al.*, 1986]:

$$R_c = \sum_{i=1}^{N} F_i R_{i,c} + E_c \qquad (2)$$

where, R_c is the apparent reflectance, at-sensor radiance, or digital number (DN) (depending on the datatype) in sensor channel c; F_i is the fraction of end-member i, $R_{i,c}$ is the radiance, reflectance or DN of end-member i in channel c; N is the number of spectral end-members, and E_c is the error for channel c of the fit of N spectral end-members. Apparent reflectance is the atmospherically corrected surface reflectance for each pixel, uncorrected for illumination differences. The fit of the linear mixture model to the spectral data in each pixel is measured by the error term E_c. Unlike the binary classification method, SMA provides a quantitative estimate of how well the model describes the multispectral image data.

The ability of the SMA model to accurately map snow cover in mountainous regions has been demonstrated by *Nolin et al.*, [1993a], using AVIRIS data, and also by *Rosenthal and Dozier*, [1993] who used Landsat TM data. In both cases, the SMA technique was found to be as accurate in mapping snow covered area as high resolution aerial photographs for discerning snow cover. *Nolin*, [1993] also demonstrated that the SMA method for snow cover mapping is relatively insensitive to illumination effects because it relies on the shape of the spectral signature of snow and other image components, rather than the magnitude of the snow signal. While this method has been found to be more accurate when surface reflectances are used, under most conditions, atmospheric correction is not required, and the unmixing can be performed using at-sensor radiances. Without atmospheric correction, each image end-member is assumed to incorporate all atmospheric effects into its spectral signature. Errors may result when the overlying atmosphere has significant spatial inhomogeneities such as large changes in optical depth from atmospheric water vapor or dust plumes. Such problems require detection using imaging spectrometer data followed by pixel-by-pixel atmospheric correction. What is critical for this mapping method is that the end-members be spectrally unique, and present in sufficient amounts to be detectable and that the sensor has the spectral and radiometric resolution needed to distinguish between the end-members [*Sabol et al.*, 1992].

Selection of end-members is the most important step in the process of spectral unmixing. End-members may be chosen from libraries of mineral and vegetation spectra [*Clark et al.*, 1993; *Grove et al.*, 1992] or they may be derived from the image data itself. For the latter case, there is typically no a priori knowledge of the number of end-members nor of the location of the purest pixels representing each end-member. It is advantageous to perform some noise reduction preprocessing to improve image end-member selection. For this, the minimum noise fraction (MNF) transform [*Green et al.*, 1988] is used in a multistep PCA to identify noise-dominated eigenimages. These noise components can be removed and the data then transformed back to the original data space. Iterative statistical analysis of the noise-reduced data is performed to identify those pixels in the multispectral image data that best represent spectrally pure pixels [*Boardman et al.*, 1995]. These automated techniques provide the information needed to identify the end-members from image data but, the final end-member selection remains a subjective process. Figure 2 shows reflectance data in Landsat TM channels 2 and 7. These images are an example of how additional spectral data can provide much needed information for scene interpretation. This scene, acquired on March 6, 1994, over Glacier National Park, Montana, has dimensions of 75 kmby 75 km. On the left, the band 2 image shows bright snow cover in the mountainous region. In the band 7 image, on the right, one can see that much of the image is influenced by cloud cover. Clouds and snow increase in contrast at longer wavelengths because of differences in their particle sizes [*Dozier*, 1989*a*]. Without sufficient spectral information, snow and clouds can be impossible to distinguish. Figure 3 shows the results of snow detection using the index-based binary classification and the SMA method. The binary classification has difficulty distinguishing clouds from snow and appears to overestimate the total snow in the image. With SMA, end-members were derived from the image using MNF for noise reduction and pixel purity identification to map the purest end-member pixels in the image. *Rosenthal and Dozier*, [1996] showed that multiple snow end-members were needed when illumination conditions varied widely. *Painter et al.*, [1998] demonstrated that when snow grain size varies over an image, the use of multiple snow end-members significantly reduces RMS error and provides a more accurate representation of snow cover. Because of the wide disparity of snow illumination conditions in the Glacier National Park TM scene, two snow end-members were needed: one which represented snow with a small solar illumination angle and one for snow with a large solar illumination angle. Other end-members included vegetation, cloud, and deep shade. In this analysis, TM

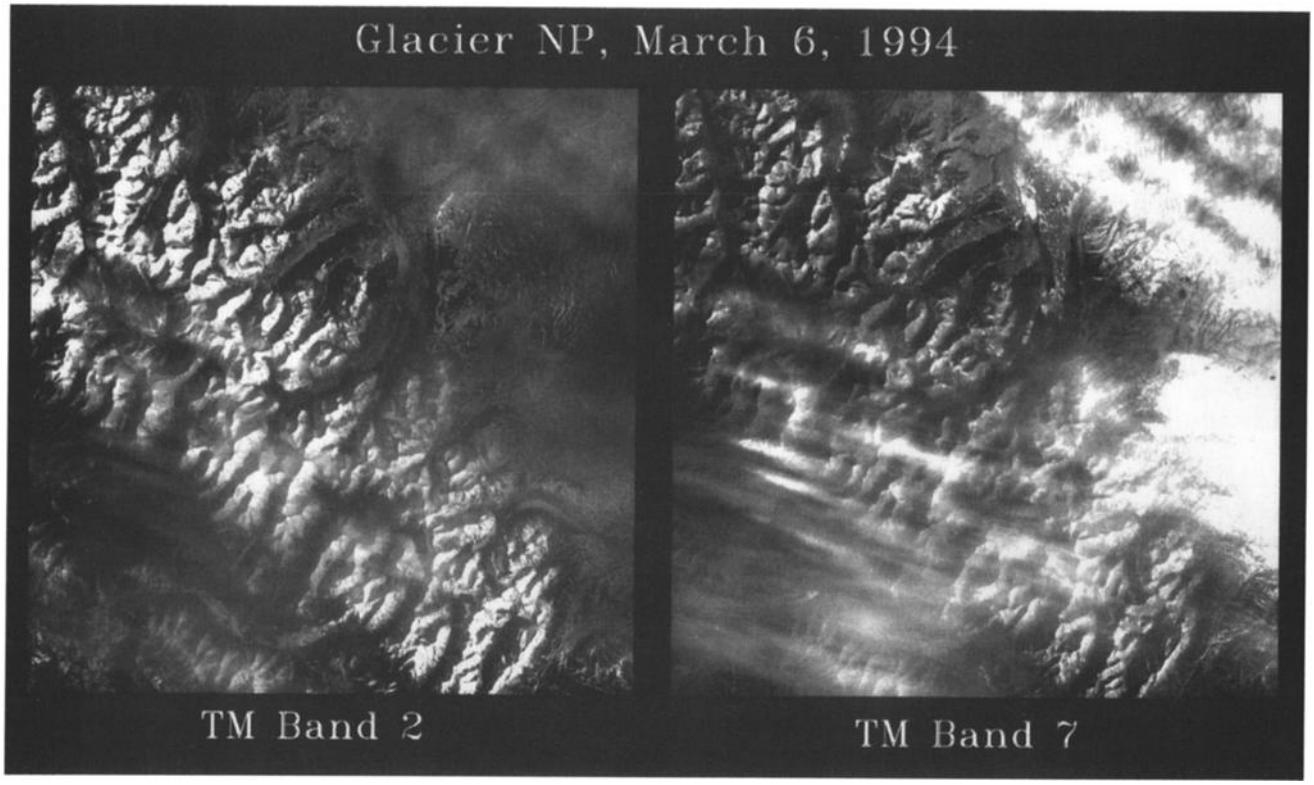

Figure 2. March 6, 1994, Landsat Thematic Mapper bands 2 (left) and 7 (right) of Glacier National Park, Montana. The image covers an area of 75 kmby 75 km. North is to the top of the image. TM band 2 appears to show extensive snow cover over the mountainous region but in TM band 7, one can see more clearly that thin clouds extend across much of the image.

bands 2-5 and 7 were used. TM band 1 was not used because it tends to saturate over snow and TM band 6 was not used because it is in the thermal region.

The SMA results show very good representation of the distribution of snow cover. Some cloudy pixels are mapped as snow but not nearly as many as the binary classification method. With both methods, slopes in deep shadow are not mapped as snow because they do not produce a sufficient signal. Also, south-facing slopes are generally mapped as having less snow than the north-facing slopes. This may be the result of incomplete spectral characterization (the two snow endmembers may not represent this type of snow). However, it is also likely that there is less snow on the south-facing slopes because of their higher insolation.

The relative accuracy of binary versus subpixel classification methods depends on the spatial resolution of the image. For coarse-resolution images in which the snow cover is heterogeneous, the SMA method is superior to the binary method. The binary classification uses a single threshold for all sensor resolutions and snow cover conditions. There is no physically based means of determining such a threshold. When image data with high spatial resolution is used and/or the surface becomes more homogeneous, the two methods will have similar levels of accuracy in snow-covered-area retrievals.

The effects of instrumental noise and calibration errors are known to influence SMA results in several ways. [*Sabol et al.*, 1992] showed that the subpixel fraction estimates are less impacted by noise as the number of bands increases. As with noise, calibration errors have a decreased effect when more bands are used. This is because each noisy measurement has less significance as the total number of measurements increases (assuming the band-to-band spectral information is uncorrelated). Thus, from the standpoint of noise/calibration-induced error, results derived from an imaging spectrometer will be less impacted by noise than those derived from a multispectral instrument such as Landsat TM. As described earlier, when using either imaging spectrometer data or multispectral data, noise reduction using the MNF transform can effectively remove noise and is a recommended step in the unmixing process.

Results for any land cover mapping method are difficult to validate and no direct measurements of snow cover or snow depth were available for this region at the time of the overpass. However, in similar studies using spectral mixture analysis over the California Sierra Nevada, the SMA results using imaging spectrometer and Landsat TM data compared very closely to estimates from high-resolution aerial photographs with a nearly 1:1 relationship [*Nolin*, 1994; *Rosenthal*, 1996; *Rosenthal and Dozier*, 1996].

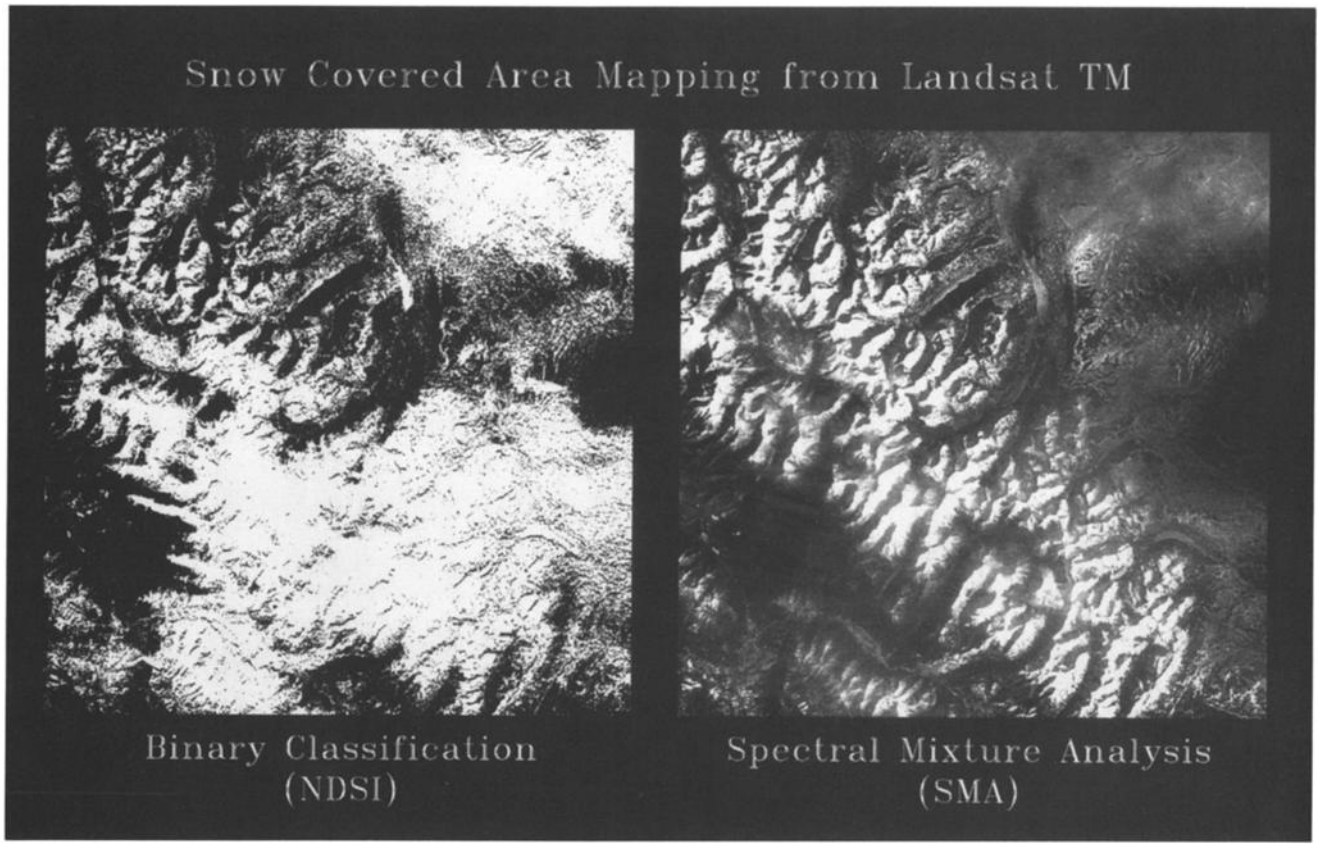

Figure 3. Multispectral snow mapping results from two different methods. The left image is the result of the binary NDSI index-based method. Cloudy regions have been mistakenly mapped as snow, and patchy snow areas have been mapped as completely snow-covered. The right image is the result of the SMA mapping subpixel method that calculates the fraction of snow, cloud, and vegetation in each pixel. This image is the snow fraction image, and dark pixels represent low or no snow cover, brighter pixels represent increasing snow cover.

3.4. Estimating Surface Layer Grain Size

3.4.1. Grain size mapping. Before proceeding with the description of the grain size mapping method, it is appropriate to discuss what is meant by the term "grain size" for remote sensing of snow. An optically equivalent sphere is used to approximate the ice crystals in the snowpack. This equivalent sphere is that which has the same volume-to-surface ratio as the irregularly shaped grains in the snowpack [*Dobbins and Jizmagian*, 1966]. Randomly oriented spheroids have been shown to be optically equivalent to spheres [*Mugnai and Wiscombe*, 1980]. Radiative transfer models allow us to relate the optical properties of snow (as measured by the spaceborne sensor) to the snowpack physical properties. In the work presented here, the grain size distribution is modeled using the optically equivalent sphere for a monodispersion of particles. Although a "natural" distribution of snow grain size is thought to resemble a lognormal distribution [*Warren*, 1982], the optically equivalent grain size is often used for computational simplicity. From stereologic analysis of snow microstructural parameters *Dozier et al.*, 1987], it has been shown that the optically equivalent grain size represents the mean grain size of the distribution [*Nolin et al.*, 1993b]. Other particle size distributions could yield the same optically equivalent grain size, but given the nature of snow grain metamorphism [*Colbeck*, 1983; *Colbeck*, 1989], it is unlikely that this would occur. For computational efficiency in performing the Mie calculations, we use a single optically equivalent/mean grain size to represent the range of snow grain sizes for a lognormal size distribution.

As described earlier, grain size affects albedo in the near-infrared region, and for relatively pure snow, it is the dominant property determining the spectrally integrated albedo. Furthermore, changes in grain size are directly attributable to temperature and temperature gradients within the snowpack [*Colbeck*, 1983].

Nolin and Dozier [1993] describe a method for using a radiative transfer model to convert snow surface reflectance in a near-infrared channel to snow grain size. Given its slope and aspect, the illumination geometry of a snow-covered pixel can be determined. For a particular illumination geometry the surface reflectance in a narrowband near-infrared channel uniquely corresponds to surface layer grain size. The spectral width of the channel is inversely proportional to the precision of

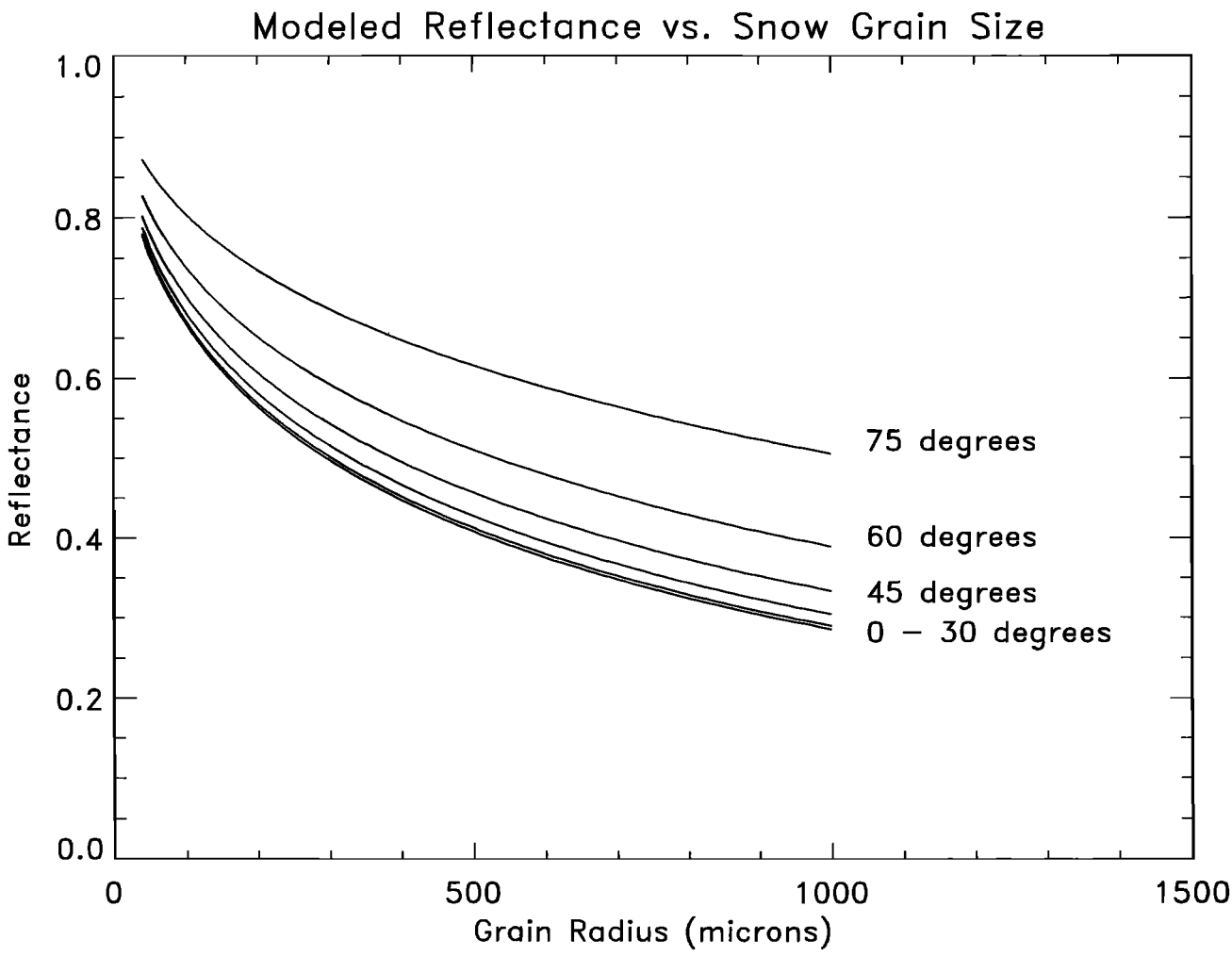

Figure 4. Snow reflectance modeled as a function of optically equivalent grain size for several illumination angles. There is little difference between the curves for illumination angles between 0° and 15°, indicating that, for relatively flat surfaces, small changes in slope will not significantly affect the grain size retrievals.

particle size determination. This narrowband inversion method is most sensitive for smaller particle sizes, such as those encountered in fresh snow and snow in cold regions such as the Greenland and Antarctic ice sheets.

In this method a single, narrow spectral band (10 nm) is used to relate scaled surface reflectance to grain size. First, the relationship between grain size and near-infrared reflectance is modeled for each illumination angle using a radiative transfer model. The discrete ordinate model [*Stamnes et al.*, 1988] was used to calculate spectral directional reflectance at $\lambda = 1.04$ μm as a function of the optically equivalent ice grain radius. Optical parameters needed for the discrete ordinate model include snowpack optical thickness, single scattering albedo, and asymmetry parameter (or a description of the scattering phase function); these are calculated from the snowpack physical properties: depth, bulk density, and equivalent grain size. Diffuse irradiance, substrate reflectance, and solar and viewing geometries are also required as model inputs. For optically semi-infinite snowpacks, both the substrate reflectance and density have a negligible effect on snowpack reflectance [*Dozier*, 1989*b*; *Bohren and Beschta*, 1979], leaving grain size as the snow property that exerts the greatest control over near-infrared reflectance.

The wavelength of 1.04 μm was chosen because it is in a spectral region where reflectance is particularly sensitive to grain radius (refer to Figure 1). A second advantage in using a band centered at that wavelength is that, for Earth, there is little atmospheric scattering or absorption, so errors due to atmospheric correction are minimized. Furthermore, the presence of typical quantities of Earth dust has very little effect on snow reflectance in that wavelength region [*Warren and Wiscombe*, 1980].

As described earlier, the relationship between modeled grain size and snowpack reflectance depends on both the solar and viewing geometries. For a nadir-viewing instrument over a flat surface, only a knowledge of the solar geometry is required to calculate the directional reflectance. However, model results show that if the illumination angle is greater than 30°(measured

from the normal to the slope), it necessary to know the angle of solar incidence before proceeding with the calculation (Figure 4).

A model-generated curve of reflectance versus grain size was fit with an exponential model of the form $r = ae^b$, where r is the calculated grain radius and a and b are coefficients used to generate a least squares fit to the model-generated data. This established a functional relationship between grain size and surface reflectance that could then be inverted to transform snowpack reflectance at 1.04 μm to an estimate of snow grain size.

To convert an image from at-sensor radiance values to snow grain size involves the following steps:

1. Perform atmospheric correction to create surface reflectance image.
2. Use subpixel snow-covered area image to mask out partially snow covered pixels.
3. Generate reflectance versus grain size curves for illumination conditions.
4. Apply inversion scheme to surface reflectance image to a grain size image.

Validation of the method was done by comparing the grain size estimates derived from narrowband reflectance data to the grain sizes in the snowpack. Snow samples were collected and later analyzed using a stereologic technique that expresses the geometrically equivalent sphere as the volume-to-surface ratio as well as the mode and standard deviation of the particle size distribution [*Perla et al.*, 1986; *Dozier et al.*, 1987, *Shi et al.*, 1993]. Size estimates derived from the images closely agree with sample grain sizes over wide range of grain sizes [*Nolin*, 1993].

A known limitation of the method is that results are valid only for those pixels that are known to be completely snow covered. Subpixel mixtures such as snow + rock + vegetation will artificially increase the estimated grain size. Thus it is highly advantageous to use the subpixel snow mapping algorithm as a preprocessing step with the grain size algorithm.

An additional limitation is that this method may not yield a unique grain size when large amounts of mineral particulates are present. If ice and mineral particles are present in a particulate mixture as separate grains or, if the ice is present as a coating on the mineral particle, Mie theory can be used to calculate their combined effective optical properties. However, even if the mineral types and the ice-mineral geometry is known, different combinations of ice and mineral particles may yield the same effective optical properties.

3.4.2. Inferring snowpack energy balance dynamics. Recent work by *Nolin and Stroeve* [1997] has demonstrated the relationship between snowpack energy balance, grain growth, and albedo. A one-dimensional model of snowpack energy and mass balance [*Jordan*, 1991] was used to calculate grain growth and that output was then used to drive a radiative transfer model that calculated spectral albedo at each time step. Changes in snowpack energy balance were seen to strongly affect albedo through grain growth, especially during periods of snowpack warming. Modeled grain size and albedo were found to closely correspond to measured values. These data show that in the near-infrared wavelengths, albedo values drop nearly 20% during a 10-day period during which grain sizes increased dramatically. This work was then spatially extended using optical remote sensing data to map albedo changes over the entire ice sheet. AVHRR satellite data were used to map monthly changes in albedo over the Greenland ice sheet during the spring and summer months. Monthly albedo images show albedo reductions of as much as 80% in the southern coastal regions. Even in areas that experience little or no melt, albedo decreases of 10–20% were common. This research demonstrates the utility of using albedo and grain size information to infer snowpack dynamics.

3.5. Snow Albedo Determination

To obtain snow albedo from remote sensing data requires that we implement a conversion scheme that incorporates a knowledge of the bidirectional reflectance distribution function (BRDF) of snow. Such a conversion scheme has been developed for use with airborne (AVIRIS) and satellite-based (AVHRR) sensors [*Nolin*, 1995, *Nolin and Stroeve*, 1997, *Stroeve et al.*, 1997] and is currently under development for the MODIS sensor.

In this research, modeling snow spectral reflectance is characterized as a multiple scattering problem [*Bohren and Barkstrom*, 1974, *Wiscombe and Warren*, 1980]. This physically based model of snow reflectance uses the equations of Mie theory to calculate the scattering properties for an optically equivalent sphere. Single particle scattering depends on the complex refractive index $m = n + ik$ (where n is the real part and k is the imaginary part) and the ratio of the particle cross-sectional area to the wavelength. This latter value is expressed as a dimensionless size parameter $x = 2\pi r/\lambda$, where r is the sphere radius and λ is the wavelength. The Disort model, with its ability to calculate the directional reflectance, is appropriate for modeling the BRDF in a multiple scattering particulate medium such as snow. Recent planetary literature has emphasized use of the [*Hapke*, 1993] model for calculating the single and multiple particle scattering properties. As yet, no systematic comparison of Hapke and the approach described here have been performed. The basic differences appear to be Hapke's inclusion of the effects of interparticle shadowing and the opposition effect [*Hapke*, 1993]. The approach described here calculates the single particle scattering properties using Mie theory and the multiple scattering properties using a discrete ordinates method. It has been shown to be sufficient for terrestrial applications; however, it may be the case that Hapke theory has advantages and these should be examined in the future.

The spectral directional-hemispherical reflectance (also referred to as the albedo) is the reflected radiance integrated over the upward hemisphere and ratioed to the direct irradiance [*Nicodemus et al.*, 1977]:

$$a_s(\mu_0) = \frac{\int_0^{2\pi}\int_0^1 \mu L(\mu,\phi)d\mu d\phi}{\mu_0 E_0} = \frac{F_\uparrow}{\mu_0 E_0} \qquad (3)$$

$L(\mu, \phi)$ is the upwelling radiance at angle θ ($\mu = \cos\theta$), azimuth ϕ. E_0 is the incident direct irradiance at the top of the snowpack at an incidence angle θ, and $F_\uparrow$ is the upward diffuse flux (integrated over all angles). Because the reflected radiance of snow depends on both solar and viewing geometries, we also need to consider the angular distribution of the reflected flux. The shape of the angular reflectance distribution is described by the anisotropic reflectance factor f, which varies with θ, θ', ϕ, and ϕ' (primed quantities are sensor viewing angles):

$$f(\theta, \theta', \phi, \phi') = \frac{\pi R_S(\theta, \theta', \phi' - \phi)}{a_s(\theta)} \quad (4)$$

R_s, the BRDF, is:

$$R_s(\theta, \theta', \phi, \phi') = \frac{dI(\theta', \phi')}{\mu_0 dF(\theta, \phi)} [\mathrm{sr}^{-1}] \quad (5)$$

where I is the solar irradiance incident at zenith θ, azimuth ϕ, F is reflected radiance, and $\mu_0 = \cos(\theta)$. The above equations all represent spectral quantities, and wavelength dependence should be considered implicit. In this paper, terminology is used that is the same as that suggested by *Warren* [1982]. Albedo refers to the directional-hemispherical reflectance. The bidirectional reflectance is the fraction of collimated light that is scattered into a particular direction; this is the reflectance quantity most often measured by satellite-based sensors.

The first step is to model both the bidirectional reflectance and albedo for a wide range of illumination and snow conditions. Snow optical properties are first calculated using Mie theory, and these spectral data are then convolved with the spectral response function for each channel. These are then used as input to the Disort model to generate a look-up table that relates the bidirectional reflectance of the snow surface to its albedo. This is done for a wide range of illumination conditions and viewing geometries. Other model inputs include sensor viewing zenith angle, relative azimuth between sun and sensor, and the relative proportions of diffuse and direct surface irradiance. The model assumes an isotropic distribution of diffuse irradiance. Reflectance-to-albedo conversion values in the look-up table are created for a wide range of snow grain sizes. The second step is to calculate the illumination and viewing geometries for each pixel using a digital elevation model, solar zenith, and sensor viewing angles. Diffuse and direct surface irradiance proportions are calculated using climatology-based estimates or measurements of atmospheric conditions. As before, the satellite image is atmospherically corrected to apparent surface bidirectional reflectance, and then nonsnow pixels are masked out. The final step is to use the look-up table relating bidirectional reflectance to albedo used to convert surface reflectance to surface albedo for each spectral band.

In the visible part of the spectrum, snow BRDF is unaffected by differences in grain size. Only the amount of dust or soot is seen to influence the results, reducing the forward scattering peak [*Nolin and Steffen*, 1995]. In the near-infrared, grain size does affect the results of the conversion (larger grains are more forward scattering). Albedo retrievals can be as much as 12% in error if an incorrect grain size is used (e.g., a radius of 50 μm rather than 1000 μm) [*Stroeve et al.*, 1997]. However, if the spectral albedo data are converted into a broadband estimate, most of these errors are eliminated because of the much higher weighting of the data from visible wavelengths (which are unaffected by grain size) [*Stroeve et al.*, 1997].

The effects of nonsphericity and internal scattering are important to consider when discussing sources of error in BRDF calculations. *Hapke* [1993] presents an overview of the effects of irregularly shaped particles on scattering. Geometric optics models using ray tracing are computationally intensive but can, in most cases provide accurate calculations. Empirical studies have also shown that non-sphericity decreases the forward scattering peak and eliminates the backscattering peak because of redirection of energy by internal scattering. Internal scatterers such as dust and bubbles can cause significant departures from Mie theory, especially when the inclusions are dark particles. For such cases it would be important to recalculate the particle scattering phase function. *McGuire* [1993] has offered a method for empirically fitting phase functions to particles in which internal scattering is important.

4. Martian Applications of Terrestrial Methods

The methods presented here have been successfully used on Earth with a variety of instruments. Multispectral sensors have been the dominant means of terrestrial mapping. In recent years, airborne visible/near-infrared imaging spectrometers have demonstrated tremendous utility in mapping subpixel mixtures, grain size, and albedo mapping. On Mars, where the dusty atmosphere and intimate mixtures of dust and ices make mapping these quantities problematic, an imaging spectrometer would be highly advantageous. With such an instrument, absorption features in reflectance spectra could be analyzed to determine particulate and ice types. Mineral-ice concentrations could be calculated using the method of *Clark and Lucey* [1984]. From these mixture reflectance spectra, classes of mineral-ice mixtures could be determined and used as end-members in spectral mixture analysis to map distributions of these mixtures in the polar regions. Knowledge of mineral concentration would also help constrain grain size calculations. Grain size estimates could also be calculated from imaging spectrometer data using the band depth [*Clark and McCord*, 1982] or band area [*Nolin*, 1993] methods.

To date, there has been no multispectral optical mapping orbiting sensor at Mars. Multispectral optical remote sensing of the polar caps would have been possible with the the Omega mapping spectrometer, the SPICAM multichannel optical spectrometer, and the SVET spectrophotometer on the ill-fated Mars 96 mission. However, with the demise of that satellite, the

Mars Orbiter Camera (MOC) flown on the Mars Global Surveyor mission is being used to produce wide-angle views of the planet's surface. The MOC is not a multispectral instrument so neither the binary nor the subpixel ice mapping methods can be used at this time. Ice cap features will only be mappable with this instrument using radiance thresholds and photogrammetric techniques. The next multispectral instrument to fly by Mars will be the Miniature Integrating Camera and Imaging Spectrometer (MICAS) on the Deep Space 1 mission, scheduled for launch in October 1998.

A recently approved payload for the European Space Agency-sponsored Mars Express Orbiter mission includes a visible and near-infrared mapping spectrometer (OMEGA) with a spatial resolution of 350 m to 1 km. This instrument is expected to have a spectral range from 0.35 μm to 5.2 μm. Its main tasks include mapping the extent of the polar caps, characterizing the temporal variability of CO_2 and H_2O ices, and identifying dust type in the icy deposits. Also on board the Mars Express satellite will be the planetary Fourier spectrometer (PFS) that will study the composition of the Martian atmosphere. These atmospheric data will allow improved atmospheric correction for better grain size and surface albedo determinations. Last, the Subsurface Sounding Radar/Altimeter (SSRA), though not an optical instrument, will be able to map ground ice in Martian crust. SSRA will measure the dielectric properties of surface and subsurface materials and be able to detect the presence of ice in soil pores. With more advanced instrumentation, many of the persistent questions regarding Martian ice can be addressed. These instruments will provide the necessary data allowing the more advanced terrestrial snow/ice mapping methods to be applied.

4.1. Mapping the Residual Ice Caps and Surface Frosts

Assuming that in the early part of the next millennium a mapping mission is carrying an imaging spectrometer, it will be feasible to perform subpixel mapping of ice and CO_2 frost extent. There may be regions where frost coverage is both dust-free and spatially homogeneous but these are not anticipated. Thus use of a pure ice frost spectrum as an end-member will not work. The SMA method implies a linear mixture of components in each pixel. Combinations of ice and dust are known to behave as nonlinear mixtures. These intimate mixtures can be of several forms: mixtures of pure particles ("salt-and-pepper"), or dust embedded in ice, coating of ice over dust, or coating of dust over ice. It may, however, be possible to partially circumvent this nonlinear mixing problem by treating the ice-mineral mixtures as end-members. One approach would be to model the spectral properties of an intimate mixture of ice and minerals as has been done by *Clark and Lucey* [1984]. A second means would be to use Mie theory to calculate the effective optical properties; this approach would work for both the multiparticle mixtures or ice-dust coatings.

SMA also assumes that the snow is optically thick and that there are no photon interactions with the underlying substrate. The optical thickness of a snowpack depends on the wavelength of observation as well as the snow properties: depth, grain size, density, and concentration of light absorbing particulates [*Warren*, 1982, *Dozier*, 1989]. Unfortunately, it is impossible for SMA to distinguish between dirty snow and thin snow, since both act as nonlinear mixtures involving dust. For Martian frosts the amount of dust is presumably large enough that the mineral-ice mixture will be optically thick even for very thin frost layers. *Clark* [1981] showed that only a small amount of dust needs to be added to a frost for it to become optically thick, even over a very dark substrate (6% reflectance).

4.2. Martian Grain Size Mapping

The single channel inversion method described earlier should be useful for grain size mapping of CO_2 frost and water ice. Rather than using a passive sensor with the Sun as the source of illumination, this method can be used with a near-infrared wavelength laser. The Mars Orbiter Laser Altimeter (MOLA) instrument can be implemented in virtually the same way as a narrowband spectrometer. This active mapping instrument is a Nd:YAG laser with a wavelength at 1.064 μm, at which not only water but CO_2 ice reflectance is sensitive to grain size. Its 160 m spot size should allow detection of relatively uniform frost-covered pixels. MOLA will be detecting not only the transmit and receive power but also the slope and aspect of the pixel. Pulse energy calibration for MOLA is about 5% [*Smith et al.*, 1998], which would be sufficient to distinguish between fine, medium and coarse sizes. The nominal resolution of the global seamless digital elevation model DEM from MOLA is 0.2° x 0.2° (approximately 9 km), which is coarse resolution for the purposes of grain size mapping. However, in the polar regions MOLA's point-to-point spacing will be about 300 m, and with its 160 m footprint, a 1 km DEM is conceivable for this region. The slope of each laser footprint is determined through analysis of the laser return pulse width. Thus all the necessary components are available for retrieving grain size from this laser altimeter. MOLA will observe the planet from a highly inclined orbit, so that the polar regions will be the most intensively mapped of any region on Mars over the 2-year mapping mission. Furthermore, unlike a spectroradiometer, a laser does not require sunlight to map the surface so grain size determinations can be made even for those times of the year when the poles are in darkness. With its high spatial resolution mapping over two annual cycles, MOLA could provide much needed information about seasonal CO_2 frost deposition, grain growth and sublimation rates.

Though originally designed for mapping water ice grain sizes, this single channel inversion method could be used for CO_2 frosts as well, since CO_2 reflectance is sensitive to grain size at the MOLA wavelength. The absorption coefficients for water ice and for CO_2 ice are of the same order of magnitude. Although CO_2 re-

flectance is more highly sensitive to grain size over the 2.0 - 4.0 μm region [*Calvin*, 1990], there is still a grain size sensitivity at 1.064 μm. Also, as Figure 4 indicates, for water ice (and presumably for CO_2 as well), the method is most sensitive for the small frost grain sizes that are likely to exist at cold Martian temperatures.

Calvin [1990] derived optical constants for CO_2 ice that showed improvements over those of *Warren* [1986]. In her examination of Mariner 9 data over the ice caps, Calvin found that the reflectance spectra most closely resemble those of large-grained CO_2 frosts (millimeter to centimeter scale) with some possible contamination by water ice and dust. However, the current CO_2 optical constants are not known well enough to be able to distinguish such mixtures. Without more accurate determinations of the CO_2 optical constants and additional data on dust concentrations, use of this inversion method is limited to relatively clean frosts containing a single ice type.

As with other surface mapping efforts, Martian dust is anticipated to be a source of error in grain size mapping. Although the concentration of Martian dust in the surface frost is unknown, it may be quite high [*Clark and McCord*, 1982]. The composition of the ice-particulate mixtures will influence the MOLA reflectivities. It may only be possible to derive grain size estimates for cases when measured 1.06 μm reflectivities are sufficiently high ($\geq$60%) that the effects of dust can be largely neglected or accounted for. Atmospheric dust in the Martian atmosphere experiences large variations as a function of both season and latitude [*Lindner*, 1990] and there can be extended periods during which there are no dust storms; for example, there have been no dust storms affecting MOLA results from the first 78 passes (J. Garvin, personal communication; 1998).

4.3. Mapping Clear-Sky Surface Albedo

In the same way that the discrete ordinates model, Disort, has been used to convert surface bidirectional reflectance to surface albedo for the Greenland ice sheet and elsewhere, a similar modeling effort could be put in place to map changes in CO_2 frost albedo. For both water ice and CO_2 frost, Disort is used to model the relationship between satellite-measured bidirectional reflectances and albedo. For this mapping effort a number of additional measurements are required: (1) atmospheric characterization to determine the relative proportions of direct and diffuse illumination at the ice surface, (2) illumination and viewing geometries, (3) grain size, and (4) dust content.

The scattering and absorbing properties of the atmosphere need to be estimated for clear-sky conditions to determine the relative proportions of direct beam and diffuse irradiance at the surface. The greater the proportion of diffuse irradiance, the more isotropic is the surface reflectance.

Illumination and viewing geometries can be determined using a DEM from the MOLA gridded elevation data. MOLA data may also provide much needed grain size estimates, allowing more accurate albedo estimation in the near-infrared region. If there are times of the year and/or portions of the frost-covered surface where the dust content is sufficiently low ($\leq$1% by weight), the near-infrared single channel inversion method can be used to estimate grain size. Even with a gross estimate of fine, medium, or coarse grain size, the near-infrared albedo could be computed using radiative transfer theory. If dust content can be estimated, the visible albedo could be computed for different types of dust/ice grain intimate mixture arrangements (e.g., "salt-and-pepper" and coatings). Ice cap albedo is a critical parameter for atmospheric circulation and global climate models, and our ability to estimate it depends on the accuracy with which we can perform atmospheric correction, estimate grain size, and know the optical properties of the dust-ice mixture.

5. Conclusions

This overview has pointed to the need for multispectral optical imagery for frost and ice mapping on Mars. The extent and variability of the Martian ice caps and their seasonal CO_2 frost covering can be mapped with only a few spectral bands distributed through the visible and near-infrared wavelengths. For instance, just a few well-situated bands (e.g., those used on the Landsat TM) provide sufficient spectral resolution for subpixel mapping. Imaging spectrometer data would provide the ability to quantify mineral-ice mixtures and to better characterize the atmosphere. These are both needed for albedo determinations, while only the former is required for subpixel frost/ice mapping. With the planned 2003 launch of the Mars Express mission carrying the OMEGA spectrometer, tests of these methods are only a few years away.

We will be able to learn more about frost dynamics as well as polar ice cap stratigraphy through adaptation of terrestrial multitemporal, multispectral mapping methods. Seasonal changes in frost-covered area will allow detection of the transition from condensing to sublimating conditions over the ice cap, thus providing important information about the annual heat budget of the polar regions.

Perhaps the most significant terrestrial mapping application is the potential use of the MOLA instrument to map grain size on the Martian polar caps. For dust concentrations less than about 1% by weight, grain size remains the dominant surface property that determines ice albedo. With its exponential response to temperature, grain size is also the physical property with the highest sensitivity to changes in the thermodynamic state of the ice. Changes in the energy balance of surface frost should be reflected in changing grain size even before the change in frost-covered area could be detected.

Surface temperature, ice type, ice-mineral mixtures, and atmospheric composition are distinctly different between Mars and Earth, so a direct application of terrestrial snow and ice mapping methods is not possible. However, expertise in mapping and interpreting terrestrial snow and ice may contribute to the collec-

tion of planetary mapping techniques. Furthermore, adaptation of appropriate methods will provide a basis for comparison of terrestrial and planetary cryospheric components.

Acknowledgments. I would like to thank Ted Scambos, Wendy Calvin and Bill Farrand for several useful discussions on planetary remote sensing. I am also grateful to Jeff Dozier, Roger Clark and Steve Drake for their careful reviews and helpful comments. This research was supported by the National Science Foundation and the National Aeronautics and Space Administration.

References

Adams, J. G., M. O. Smith, and P. E. Johnson, Spectral mixture modeling: A new approach to analysis of rock and soil types at the Viking Lander 1 site, *J. Geophys. Res., 91,* 8098-8112, 1986.

Barlow, L. K., J. W. C. White, R. G. Barry, J. C. Rodgers, and P. M. Grootes, The North Atlantic oscillation signature and deuterium excess signals in the Greenland Ice Sheet Project 2 ice core, 1840-1970, *Geophys. Res. Lett., 20,* 2901-2904, 1993.

Barry, R. G., The cryosphere and climate change, in *Detecting the Climatic Effects of Increasing Carbon Dioxide,* DOE/ER-0235, edited by M. C. MacCracken and F. M. Luther, pp. 109-141, U.S. Dep. of Energy, Washington, D.C., 1985.

Boardman, J. W., F. A. Kruse and R. O. Green, Mapping target signatures via partial unmixing of AVIRIS data, *Summaries of the Fifth Annual JPL Airborne Earth Science Workshop, 95-1,* 23-26, 1995.

Bohren, C. F., and B. R. Barkstrom, Theory of the optical properties of snow, *J. Geophys. Res., 79,* 4527-4535, 1974.

Bohren, C. F., and R. L. Beschta, Snowpack albedo and snow density, Cold Reg. Sci. Technol. *1,* 47-50, 1979.

Calvin, W. M., Additions and corrections to the absorption coefficients of CO_2 ice: Applications to the Martian south polar cap, *J. Geophys. Res., 95,* 14,743-14,750, 1990.

Clark, R. N., The spectral reflectance of water-mineral mixtures at low temperatures, *J. Geophys. Res., 86,* 3074-3086, 1981.

Clark, R. N., and P. G. Lucey, Spectral properties of ice-particulate mixtures and implications for remote sensing, 1, Intimate mixtures, *J. Geophys. Res., 89,* 6341-6348, 1984.

Clark, R. N., and T. B. McCord, Mars residual north polar cap: Earth-based spectroscopic confirmation of water ice as a major constituent and evidence for hydrated minerals, *J. Geophys. Res., 87,* 367-370, 1982.

Clark, R. N., and T. L. Roush, Reflectance spectroscopy: Quantitative analysis techniques for remote sensing applications, *J. Geophys. Res., 89,* 6329-6340, 1984.

Clark, R. N., F. P. Fanale, and A. P. Zent, Frost grain size metamorphism: Implications for remote sensing of planetary surfaces, *Icarus, 56,* 233-245, 1983.

Clark, R. N., G. A. Swayze, A. Gallagher, T. V. V. King, and W. M. Calvin, The U. S. Geological Survey digital spectral library: Version 1: 0.2 to 3.0 μm, *U. S. Geol. Surv. Open File Rep. 93-592,* 1993.

Colbeck, S. C., Theory of metamorphism of dry snow, *J. Geophys. Res., 88,* 5475-5482, 1983.

Colbeck, S. C., Snow-crystal growth with varying surface temperatures and radiation penetration, *J. Glaciol., 35,* 23-29, 1989.

Dobbins, R. A., and G. S. Jizmagian, Optical scattering cross sections for polydispersions of dielectric spheres, *J. Opt. Soc. Am., 56,* 1345-1350, 1966.

Dozier, J., Spectral signature of alpine snow cover from the Landsat Thematic Mapper, *Remote Sens. Environ., 28,* 9-22, 1989a.

Dozier, J., Remote sensing of snow in the visible and near-infrared wavelengths, in *Theory and Applications of Optical Remote Sensing,* edited by G. Asrar, pp. 527-547, John Wiley and Sons, New York, 1989b.

Dozier, J., and D. Marks, Snow mapping and classification from Landsat Thematic Mapper data, *Ann. Glaciol., 9,* 1-7, 1987.

Dozier, J., R. E. Davis, and R. Perla, On the objective analysis of snow microstructure, in *Avalanche Formation, Movement and Effects,* edited by G. Salm and H. Gubler, *IAHS Publ. 162,* 46-59, 1987.

Farmer, C. B., D. W. Davies and D. D. LaPorte, Mars: Northern summer ice cap-water vapor observations from Viking 2, *Science, 194,* 1339-1341, 1976.

Gillespie, A. R., M. O. Smith, J. B. Adams, S. C. Willis, A. F. Fischer, and D. E. Sabol, Interpretation of residual images: Spectral mixture analysis of AVIRIS images, Owens Valley California, in *Proceedings of the Second Annual JPL Airborne Earth Science Workshop, 90-54,* 243-270, 1990.

Green, A. A., M. Berman, P. Switzer, and M. D. Craig, A transformation for ordering multispectral data in terms of image quality with implications for noise removal, *IEEE Trans. Geosci. Remote Sens., 26,,* 65-74, 1988.

Grove, C. I., S. J. Hook, and E. D. Paylor, Laboratory reflectance spectra of 160 mineral, 0.4 to 2.5 micrometers. *JPL Publ., 92-2,* 1992.

Haberle, R. M., and B. M. Jakosky, Sublimation and transport of water from the north residual polar cap on Mars, *J. Geophys. Res., 95,* 1423-1437, 1990.

Hall, D. K., G. A. Riggs, and V. V. Salomonson, Development of methods for mapping global snow cover using Moderate Resolution Imaging Spectroradiometer data, *Remote Sens. Environ., 54,* 127-140, 1995.

Hapke, B., *Theory of Reflectance and Emittance Spectroscopy, Topics in Remote Sens. 3,* Cambridge Univ. Press, New York, 1993.

Howard, A. D., J. A. Cutts, and K. R. Blasius, Stratigraphic relationships within Martian polar cap deposits, *Icarus, 50,* 161-215, 1982.

Jakosky, B. M., and C. B. Farmer, The seasonal and global behavior of water vapor in the Mars atmosphere: Complete global results of the Viking atmospheric water vapor detector experiment, *J. Geophys. Res., 87,* 2999-3019, 1982.

Johnsen, S. J., H. B. Clausen, and W. Dansgaard, Irregular glacial interstadials recorded in a new Greenland ice core, *Nature, 359,* 311-312, 1997.

Jordan, R., A one-dimensional temperature model for a snow cover: Technical documentation for SNTHERM.89, *Spec. Rep. 91-16,* U. S. Army Corps of Eng., Cold Regions Res. and Eng. Lab., Hanover, N. H., 1991.

Kieffer, H. H., H_2O grain size and the amount of dust in Mars' residual north polar cap, *J. Geophys. Res., 95,* 1481-1493, 1990.

Kieffer, H. H., S. C. Chase Jr., T. Z. Martin, E. D. Miner, and F. D. Palluconi, Martian north polar summer temperatures: Dirty water ice, *Science, 194,* 1341-1344, 1976.

Kumai, M., Identification of nuclei and concentrations of chemical species in snow crystals sampled at the South Pole, *J. Atmos. Sci., 33,* 833-841, 1976.

Lawton, W. H., and E. A. Sylvestre, Self modeling curve resolution, *Technometrics, 13,* 617-633, 1971.

Lindner, B. L., The Martian polar cap: Radiative effects of ozone, clouds, and airborne dust, *J. Geophys. Res., 95,* 1367-1379, 1990.

McGuire, A., Experimental investigation of light scattering

by large irregularly shaped particles, Ph. D. thesis, Univ. of Pittsburgh, Pittsburgh, Pa., 1993.

Mellon, M. T., Limits on the CO_2 content of the Martian polar deposits, *Icarus, 124,* 268-279, 1996.

Mellon, M. T., Small-scale polygonal features on Mars: Seasonal thermal contraction cracks in permafrost, *J. Geophys. Res., 102,* 25,617-25,628, 1997.

Mellon, M. T., and B. M. Jakosky, The distribution and behavior of Martian ground ice during past and present epochs, *J. Geophys. Res., 100,* 11,781-11,799, 1995.

Mellon, M. T., B. M. Jakosky, and S. E. Postawko, The persistence of equatorial ground ice on Mars, *J. Geophys. Res., 102,* 19,357-19,372, 1997.

Mugnai, A. and W. J. Wiscombe, Scattering of radiation by moderately nonspherical particles, *J. Atmos. Sci., 37,* 1291-1307, 1980.

Mustard, J. F., and C. M. Pieters, Photometric phase functions of common geologic minerals and applications to quantitative analysis of mineral mixture reflectance spectra, *J. Geophys. Res., 94,* 13,619-13,634, 1989.

Nicodemus, F. E., J. C. Hsia, J. J. Richmond, I. W. Ginsberg, and T. Limperis, Geometrical considerations and nomenclature for reflectance, *Tech. Rep. Monogr. 160,* Natl. Bur. of Stand., Gaithersburg, Md., 1977.

Nolin, A. W., Radiative heating in alpine snow, Ph.D. thesis, Univ. of Calif., Santa Barbara, 1993.

Nolin, A. W., Snowcover mapping with the Airborne Visible/Infrared Imaging Spectrometer, in *Proceedings of the International Geoscience and Remote Sensing Symposium '94, 94CH3378-7,* pp. 2081-2083, Inst. of Electr. and Electron. Eng., New York, 1994.

Nolin, A. W., and J. Dozier, Estimating snow grain size using AVIRIS data, *Remote Sens. Environ., 44,* 232-238, 1993.

Nolin, A. W., Snow albedo from BRDF parameterizations, *Eos Trans. AGU, 76* (46), Fall Meet. Suppl., F185, 1995.

Nolin, A. W., and J. C. Stroeve, The changing albedo of the Greenland ice sheet: Implications for climate modeling, *Ann. Glaciol., 25,* 51-57, 1997.

Nolin, A. W., J. Dozier, and L. A. K. Mertes, Mapping alpine snow using a spectral mixture modeling technique, *Ann. Glaciol., 17,* 121-124, 1993a.

Nolin, A. W., J. Shi, and J. Dozier, Characterization of snow grain size in the near-infrared and microwave wavelengths, in *Proceedings of the IEEE Combined Optical-Microwave Earth and Atmosphere Sensing Symposium,* pp. 51-54, Inst. Electr. and Electron. Eng., New York, 1993b.

Paige, D. A., The thermal stability of near-surface ground ice on Mars, *Nature, 356,* 43-45, 1992.

Paige, D. A., and A. P. Ingersoll, Annual heat balance of Martian polar caps: Viking observations, *Science, 228,* 1160-1168, 1985.

Painter, T. H., D. A. Roberts, R. O. Green, and J. Dozier, The effect of grain size on spectral mixture analysis estimates of snow-covered area from AVIRIS data, *Remote Sens. Environ., 65,* 320-332, 1998.

Perla, R., J. Dozier, and R. E. Davis, Preparation of serial sections in dry snow specimens, *J. Microsc., 142,* 111-114, 1986.

Pollack, J. B., R. M Haberle, J. Schaeffer, and H. Lee, Simulations of the general circulation of the Martian atmosphere, 1., Polar processes, *J. Geophys. Res., 95,* 1147-1473, 1990.

Roberts, D. A., M. O. Smith, and J. B. Adams, Green vegetation, nonphotosynthetic vegetation, and soils in AVIRIS data, *Remote Sens. Environ., 44,* 255-269, 1993.

Robinson, D. A., and K. F. Dewey, Recent secular variations in Northern Hemisphere snow cover, *Geophys. Res. Lett., 17,* 1557-1560, 1990.

Rosenthal, W., Mapping montane snow cover at subpixel resolution from the Landsat Thematic Mapper, M. S. thesis, Univ. of Calif., Santa Barbara, 1993.

Rosenthal, W., Estimating alpine snow cover with unsupervised spectral unmixing, in *Proceedings of the International Geoscience and Remote Sensing Symposium '96,* pp. 2252-2254, Inst. of Electr. and Electron. Eng., New York, 1996.

Rosenthal, W., and J. Dozier, Automated mapping of montane snow cover at subpixel resolution from the Landsat Thematic Mapper, *Water Resour. Res., 32,* 115-130, 1996.

Royer, A., M. DeAngelis, and J. R. Petit, A 30,000 year record of physical and optical properties of microparticles from an East Antarctic ice core and implications for paleoclimate reconstruction models, *Clim. Change, 5,* 381-412, 1983.

Sabol, D. E., J. B. Adams, and M. O. Smith, Quantitative subpixel spectral detection of targets in multispectral images, *J. Geophys. Res., 97,* 2659-2672, 1992.

Shi, J., R. E. Davis, and J. Dozier, Stereological determination of dry snow parameters for discrete microwave modeling, *Ann. Glaciol., 17,* 295-299, 1993.

Shook, K., D. M. Gray, and J. W. Pomeroy, Temporal variation in snowcover area during melt in prairie and alpine environments, *Nordic Hydrol., 24,* 183-198, 1993.

Smith, D. E., et al., Topography of the northern hemisphere of Mars from the Mars Orbiter Laser Altimeter, *Science, 279,* 1686-1692, 1998.

Stamnes, K., S. Tsay, W. Wiscombe, and K. Jayaweera, Numerically stable algorithm for discrete-ordinate-method radiative transfer in multiple scattering and emitting layered media, *Appl. Opt., 27,* 2502-2509, 1988.

Stroeve, J. C., A. W. Nolin, and K. Steffen, Comparison of AVHRR-derived and in situ surface albedo over the Greenland ice sheet, *Remote Sens. Environ., 62,* 262-276, 1997.

Warren, S. G., Optical properties of snow, *Rev. Geophys., 20,* 67-89, 1982.

Warren, S. G., Optical constants of carbon dioxide ice, *Appl. Opt., 25,* 2650-2674, 1986.

Warren, S. G., and W. J. Wiscombe, A model for the spectral albedo of snow, II. Snow containing atmospheric aerosols, *J. Atmos. Sci., 37,* 2734-2745, 1980.

White, D. E., J. W. C. White, and L. K. Barlow, Reconstructing annual and seasonal climatic responses from volcanic events since A. D. 1270 as recorded in the deuterium signal from the Greenland Ice Sheet Project 2 ice core, *J. Geophys. Res., 102,* 19,683-19,684, 1997.

Wiscombe, W. J., and S. G. Warren, A model for the spectral albedo of snow, I. Pure snow, *J. Atmos. Sci., 37,* 2712-2733, 1980.

Yang, Q., P. A. Mayewski, and S. Whitlow, Major features of glaciochemistry over the last 110,000 years in the Greenland Ice Sheet Project 2 ice core, *J. Geophys. Res., 102,* 23,289-23,298, 1997.

A. W. Nolin, CIRES/NSIDC, Campus Box 449, University of Colorado, Boulder, CO 80309-0449. (e-mail: nolin@spectra.colorado.edu)

(Received November 26, 1997; revised June 8, 1998; accepted June 10, 1998.)